ACS BIO & MED CHEM Au
AN OPEN ACCESS JOURNAL OF THE AMERICAN CHEMICAL SOCIETY

pubs.acs.org/biomedchemau
Article

New Catalytic Residues and Catalytic Mechanism of the RNase T1 Family

Katsuki Takebe, Mamoru Suzuki, Yumiko Hara, Takuya Katsutani, Naomi Motoyoshi, Tadashi Itagaki, Shuhei Miyakawa, Kuniaki Okamoto, Kaori Fukuzawa, and Hiroko Kobayashi*

Cite This: ACS Bio Med Chem Au 2024, 4, 257−267
Read Online
ACCESS | Metrics & More | Article Recommendations | Supporting Information

ABSTRACT: The ribonuclease T1 family, including RNase Po1 secreted by *Pleurotus ostreatus*, exhibits antitumor activity. Here, we resolved the Po1/guanosine-3′-monophosphate complex (3′GMP) structure at 1.75 Å. Structure comparison and fragment molecular orbital (FMO) calculation between the apo form and the Po1/3′GMP complex identified Phe38, Phe40, and Glu42 as the key binding residues. Two types of the RNase/3′GMP complex in RNasePo1 and RNase T1 were homologous to Po1, and FMO calculations elucidated that the biprotonated histidine on the β3 sheet (His36) on the β3 sheet and deprotonated Glu54 on the β4 sheet were advantageous to RNase activity. Moreover, tyrosine (Tyr34) on the β3 sheet was elucidated as a crucial catalytic residues. Mutation of Tyr34 with phenylalanine decreased RNase activity and diminished antitumor efficacy compared to that in the wild type. This suggests the importance of RNase activity in antitumor mechanisms.

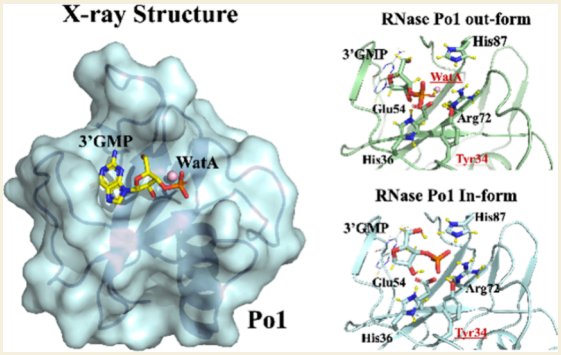

KEYWORDS: *RNase, crystal structure, fragment molecular orbital method, interfragment interaction energy, antitumor activity, RNase activity*

1. INTRODUCTION

The ribonuclease T1 family, found in fungi and bacteria, includes a low-molecular-weight enzyme that hydrolyzes single-stranded RNA using a 2′,3′-cyclic phosphate intermediate at the 3′ end of oligonucleotides.[1] RNase Po1, a member of the RNase T1 family, is secreted by an edible mushroom, *Pleurotus ostreatus*.[2] It is an 11 kDa enzyme sharing 40% homology in the amino acid sequence with RNase T1, which is one of the most representative RNase enzymes in the T1 family. Both RNases are neutral and specific in their function.[2,3] Po1, an alkaline protein in terms of the theoretical isoelectric point (PI), exhibits antitumor activity against neuroblastoma and leukemia cells.[4] In the RNase T1 family, α-sarcin differs from Po1 in structural properties in that the α-sarcin protein secreted from *Aspergillus giganteus* is alkaline in PI and exhibits antitumor activity; however, it is large (17 kDa) and has low amino acid sequence homology with T1.[3,5,6] The (α+β)-type structure of the RNase T1 family features a highly conserved active center[3,7−12] containing catalytic residues crucial for its catalytic activity (Figure 1). While His40, Glu58, Arg77, and His92 in RNase T1 were considered potential catalytic residues, other studies have suggested that Glu58, instead of His40, may serve as a common base catalyst.[12−15] Despite these efforts, the mechanism and specific catalytic residues involved in the RNase activity of the T1 family remain unclear. Research on the antitumor activity of RNase has focused on α-sarcin and onconase, both demonstrating strong antitumor activity.[16−18] Their cationic surfaces facilitate binding to the plasma membrane for internalization. Po1 shares a similar cationic surface, believed to be crucial for its antitumor activity.[3] While cytotoxic RNases target intercellular RNA, the link between RNase activity and antitumor activity remains unknown. This study aimed to clarify the catalytic residues and mechanism involved in RNase activity within the RNase T1 family and explore the relationship between RNase activity and antitumor effects.

We present the structure of the Po1/guanosine-3′-monophosphate (3′GMP) complex, identifying the key residues for 3′GMP base recognition, and discussing the mechanism of water-mediated RNA binding. We highlighted a new catalytic residue, Tyr34, and analyzed its structure and interactions using the fragment molecular orbital (FMO) method,[19] a quantum chemical calculation method. Furthermore, a comparison between mutant Po1 (Tyr34/Phe34) with

Received: June 28, 2024
Revised: September 10, 2024
Accepted: September 10, 2024
Published: September 20, 2024

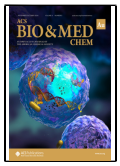

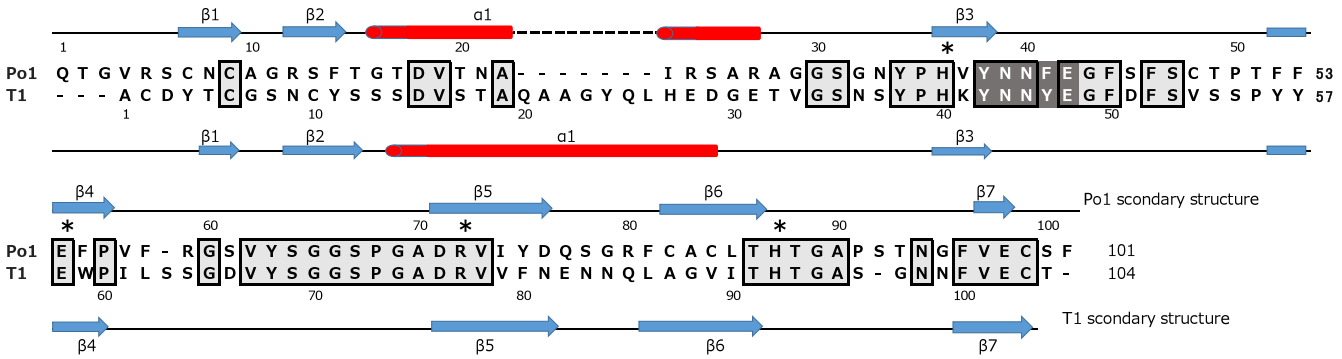

Figure 1. Primary and secondary structures of RNase Po1 and RNase T1. Po1, RNase Po1; T1, RNase T1. Sequences in common are enclosed in boxes. Numbers above and below the matrix represent RNase Po1 and RNase T1 numbering, respectively. *Catalytic site. The base recognition site is shaded. Secondary structures are denoted as follows: α1, α-helix; βn, β-strand structure.

reduced RNase activity and wild-type Po1 indicated a relationship between RNase activity and antitumor activity.

2. EXPERIMENTAL PROCEDURES

Enzymes

RNase Po1 was expressed in *Escherichia coli*. The cDNA was ligated into the expression vector pET-pel-Po1, constructed following the procedure by Huang et al.[20] from pET22b (Novagene, Darmstadt, Germany), and subsequently transferred to *E. coli* BL21 (DE3) pLysS (Novagene). The cells were cultured in Terrific broth at 25 °C for 7 days and supplemented with 100 μg/mL ampicillin. Subsequently, 1 mL of 0.5 M isopropyl β-D-thiogalactopyranoside (IPTG; Wako Pure Chemical Industries, Osaka, Japan) was added to 1 L of the medium to yield a final concentration of 0.5 mM. The supernatant of the culture was used for subsequent purification steps, which included fractionating with 90% saturated ammonium sulfate and collecting the precipitate by centrifugation at 16,900 × *g* for 30 min at 4 °C. The precipitate was resuspended in 10 mM acetate buffer (pH 6.0) and dialyzed overnight against deionized water. The dialysate was heated to 60 °C for 10 min and then rapidly cooled in ice-cold water for 10 min. The precipitate was recovered by centrifugation at 16,900 × *g* for 30 min. Subsequent purification steps were performed using previously described protocols.[3] The mutant Po1 was expressed in the same way as the RNase Po1. The cells were cultured in Terrific broth at 25 °C for 4 days, and the supernatant of the culture was used for subsequent purification steps using column chromatography in the following order: Sp-Toyopearl column (3 × 30 cm, TOSOH, Tokyo, Japan) at pH 5.0, Ultrogel AcA54 column (3 × 180 cm, GE Healthcare) at pH 7.0, DEAE-Toyopearl column (3 × 30 cm, TOSOH, Tokyo, Japan) at pH 7.0, and Heparin-Sepharose column (1 × 20 cm, GE Healthcare) at pH 4.5. Finally, the RNase-active fractions of mutant Po1 were subjected to gel filtration using an Ultrogel AcA54 column (1.5 × 180 cm, GE Healthcare) at pH 7.0.

Enzyme Assay

RNase activity was measured as previously described using yeast RNA (Marine Biochemicals, Tokyo, Japan) as the substrate at pH 7.5 and 37 °C.[21]

Protein Concentration

The protein concentration of the final enzyme preparation was measured colorimetrically and quantified using a Pierce BCA Protein Assay Kit (Thermo Fisher Scientific, Waltham, Massachusetts) with bovine serum albumin as a standard.

Tricine-Sodium Dodecyl Sulfate-Polyacrylamide Gel Electrophoresis (SDS-PAGE)

Tricine-SDS-PAGE was performed using a 15% polyacrylamide gel using Schägger's method.[22,23] Proteins on the gel were stained by using silver staining.

Evaluation of Antiproliferative Activity of RNase Po1 and Mutant Po1 of HL-60 Cells via 3-(4,5-Dimethylthiazol-2-yl)-2,5-diphenyltetrazolium Bromide (MTT) Assay

Anticell proliferative activity was measured using human leukemia cells (HL-60 cells) using the method followed by Nitta et al.[24] The HL-60 cells were cultured in RPMI 1640 (Invitrogen, Carlsbad, CA) supplemented with 10% fetal calf serum (Bio West, Strasbourg, France). The cells were collected via centrifugation, subsequently suspended in the medium, and diluted to 3×10^5 cells/mL. The cell suspension (200 μL) was added to each well of a 96-well plate. Subsequently, 10 μL of various RNase Po1 or mutant Po1 concentrations previously filtered with a Millipore filter (Millex-GV Billerica, MA, USA) was added.

Viable cells were counted using the MTT assay after 72 h of incubation at 37 °C under 5% CO_2. After 10 μL of 0.5% MTT solution (Wako Pure Chemical Industries, Ltd.) was added in the well, incubation was continued for a further 2−3 h at 37 °C and 5% CO_2.

Subsequently, the absorbance at 570 nm was measured. The inhibition activity of cell proliferation in the cells was calculated as the percentage decrease of the increase in cell number without mutant Po1.

Crystallization of RNase Po1 Complexed with 3′GMP

For crystallization, purified RNase Po1 was dissolved in a buffer [20 mM Tris (hydroxymethyl) aminomethane-HCl (Wako Pure Chemical Industries, Osaka, Japan) (pH 7.5)] and adjusted to 10 mg/mL. Subsequently, RNase Po1 was mixed at a molar ratio of 1:5 with 3′GMP (Sigma Chemical. Co., St. Louis, USA) on ice. RNase Po1 complexed with 3′GMP was crystallized at 20 °C by using the hanging drop vapor diffusion method. An initial crystal was obtained using specific conditions [60% (v/v) Tacsimate (pH 7.0) and 0.1 M BIS-TRIS propane (pH 7.0)] in SaltRx (Hampton Research, Aliso Viejo, CA). Drops were placed over a well containing 500 μL of a reservoir solution. Crystals suitable for data collection were obtained in drops containing 0.5 μL of protein solution (10 mg/mL) mixed with 0.5 μL of reservoir solution [50% Tacsimate (pH 7.0)] after 5 days.

Data Collection and Determining the Structure

Diffraction data were measured at 100 K and a wavelength of 1.100 Å by using a PILATUS 2M-F detector on beamline BL-1A at the Photon Factory, Tsukuba, Japan. Data from a single crystal were integrated and scaled using HKL2000.[25] The structure was determined via molecular replacement with phaser_MR[26] using RNase Po1's structure (PDB code 3WHO) as a search model. Structure refinement was performed using Refmac5[27] and Phenix.[28] The molecular model was manually corrected in the electron density map using Coot.[29] (Table 1).

https://doi.org/10.1021/acsbiomedchemau.4c00046
ACS Bio Med Chem Au 2024, 4, 257−267

Model Preparation

We computed two binding forms of Po1 and T1 (Figure 2A–D). The form is illustrated by the RNase T1/3′GMP complex (PDBID: 6GSP), where the phosphate is bound to the deep region of the active center. On the other hand, the out-form is depicted by the RNase Po1/3′GMP complex (PDBID: 3WR2), where the phosphate is bound to the shallow region of the active center.

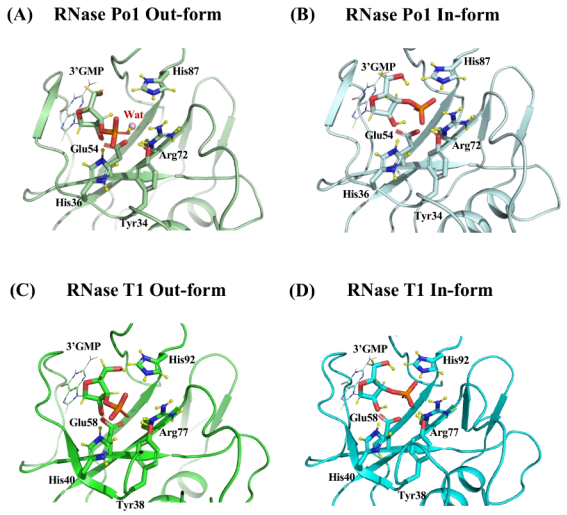

Figure 2. Modeling of the in- and out-forms of Po1/3′GMP and T1/3′GMP. (A) Out-form of the Po1/3′GMP complex. The side chain of Glu54 was the deprotonated state of a carboxylate group. This model was derived from PDBID: 3WR2. (B) In-form of the Po1/3′GMP complex The side chain of Glu54 was the protonated state of a carboxylate group. This model was derived from PDBID: 3WR2. (C)In-form of the T1/3′GMP complex. The side chain of Glu58 was the protonated state of a carboxylate group. This model was derived from PDBID: 6GSP. (D) Out-form of the T1/3′GMP complex. The side chain of Glu58 was the deprotonated state of a carboxylate group. This model was derived from PDBID: 4GSP.

The out-form of Po1/3′GMP, in-form of T1/3′GMP, and out-form of T1/3′GMP were modeled using X-ray crystallographic structures. Contrastingly, the in-form of Po1/3′GMP was modeled by combining the Po1/3′GMP and T1/3′GMP complex.

Design of the Modeling Structure of Po1 and T1

In-Form of Po1/3′GMP. First, the structures of the Po1/3′GMP (PDB ID: 3WR2) and T1/3′GMP (PDB ID: 6GSP) complexes were superimposed on the main chain, and the 3′GMP in the Po1/3′GMP complex was replaced by the T1/3′GMP complex. Subsequently, water molecules in the Po1/3′GMP complex were removed within 2.0 Å of the 3′GMP. The side chain of the carboxylate group of Glu54 was deprotonated (Figure 2A).

Out-Form of Po1/3′GMP. The crystal structure of Po1/3′GMP (PDB ID: 3WR2) was used as the initial structure (Figure 2B).

In-Form of T1/3′GMP. The crystal structure of T1/3′GMP (PDB ID:6GSP) was used as the initial structure. The side chain of the carboxylate group of Glu58 was deprotonated (Figure 2C).

Out-Form of T1/3′GMP. Subsequently, we removed the guanosine-2′,3′-cyclophosphorothioate (SGP) from the crystal structure of T1/3′GMP and the SGP complex and used it as the initial structure (Figure 2D).

Structure Optimization and Protonation

All the models were protonated using Protonate 3D, available in the Molecular Operating Environment (MOE) software package.[30] The models of the in-form of Po1/3′GMP, in-form of T1/3′GMP, and out-form of T1/3′GMP were optimized from the ligand to surrounding 4.5 Å amino acid residues with a constraint (tether = 0.5), followed by hydrogen optimization. Contrastingly, the out-form model of Po1/3′GMP was optimized using only all hydrogens with a constraint (tether = 0.5). All optimizations were performed under the AMBER10: EHT force field.[31]

FMO Calculation

All FMO calculations[19] were performed on the Fugaku supercomputer using the ABINIT-MP program[32] at the second-order Møller–Plesset perturbation theory (MP2),[33,34] with a 6-31G* basis set. In this calculation, all proteins were divided by the amino acid residues, and the ligand (3′GMP) was divided into base and sugar–phosphate fragments.[32]

In FMO calculation, E_{total}, which was the total energy of the molecule, was expressed by the following equation using E_i', which represents the energy of the monomer fragment without environmental electrostatic potential, and $\Delta\tilde{E}_{ij}$, which represents the two-body interaction energy between fragments i and j.

$$E_{total} = \sum_i E_i' + \sum_{i>j} \Delta\tilde{E}_{ij}$$

Herein, $\Delta\tilde{E}_{ij}$ is known as IFIE. IFIE represents the sum of the following four components as obtained using PIEDA (pair interaction energy decomposition analysis):[35] $\Delta\tilde{E}^{ES}$, electrostatic; $\Delta\tilde{E}^{EX}$, exchange-repulsion; $\Delta\tilde{E}^{CT+mix}$, charge transfer with higher-order mixed terms; and $\Delta\tilde{E}^{DI}$, dispersion interaction terms. In other words, IFIE is the sum of the energies of these four energy terms.

$$\Delta\tilde{E}_{ij} = \Delta\tilde{E}_{ij}^{ES} + \Delta\tilde{E}_{ij}^{EX} + \Delta\tilde{E}_{ij}^{CT+mix} + \Delta\tilde{E}_{ij}^{DI}$$

The hydrogen bond interaction was mainly composed of ES and CT +mix terms. The CH/π and π–π interactions were mainly composed of the DI term.[36]

3. RESULTS AND DISCUSSION

Purification and Crystallization of RNase Po1 and Determination of Its Structure

Expression of RNase Po1 in *E. coli* provided approximately 35,000 units (~17 mg) of RNase Po1 in 2 L of culture supernatant. RNase Po1 was homogeneous, as shown by SDS-PAGE (Figure 3(1)). The crystals of the Po1/3′GMP complex were obtained in the space group $P2_12_12_1$ with the following

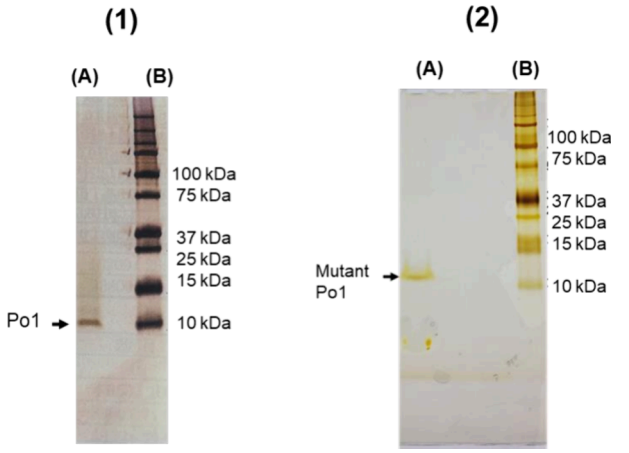

Figure 3. Tricine-sodium dodecyl sulfate (SDS)-polyacrylamide gel electrophoresis (PAGE) (15%) of RNase Po1 and the mutant Po1. Silver staining of the Tricine-SDS-Page (15%) of the RNase Po1(1) and mutant Po1(2), where (A) RNase Po1 or the mutant Po1 and (B) molecular protein makers are indicated.

https://doi.org/10.1021/acsbiomedchemau.4c00046
ACS Bio Med Chem Au 2024, 4, 257–267

unit lattice parameters a, b, c (Å) = 55.07, 95.87, 106.22. The structure was determined at a resolution of 1.75 Å. The Po1/3′GMP complex comprises six molecules in the asymmetric unit lattice. The final refinement statistics were R_{work} = 0.169 and R_{free} = 0.211. Crystallographic statistics are summarized in Table S1.

Crystal Structure Analysis of Po1/3′GMP

The overall Po1/3′GMP structure formed an (α+β)-type structure and consisted of a 3.5-turn α-helix (RNase Po1: residues 16−27) running like a backbone under the molecule and seven β-sheets (RNase Po1: residues 7−9, 12−14, 36−38, 52−56, 71−76, 82−86, 97−98) (Figure 4A). In the Po1/3′GMP structure, three intramolecular disulfide bonds were identified (Cys7−Cys84, Cys9−Cys99, Cys48−Cys82), mirroring the same positions observed in the apo form.[3] The guanosine base binding site encompasses the β3-β4 (comprising Tyr38, Asn39, Asn40, Phe41, and Glu42) and β6-β7 (containing Asn93). The aromatic Tyr38 and Phe41 rings are stacked with guanine bases (Figure 4B). The catalytically active amino acid residues of Po1 (His36, Glu54, Arg72, and His87) are the same as those in the T1/3′GMP structure (His40, Glu58, Arg77, and His92) and are conserved at the same position. However, His87 of RNase Po1/3′GMP could not be bonded by hydrogen directly with the phosphate group of 3′GMP due to the 6.4 Å distance. This phosphate group forms hydrogen bonds with adjacent Arg5 and Arg80 of other Po1 molecules in the crystal, potentially contributing to stabilizing the phosphate position through crystal packing effects. In the T1/3′GMP complex, the phosphate group of the 3′GMP binding position has been reported in two types of structures regardless of the crystal packing.[37] This phosphate position is discussed below.

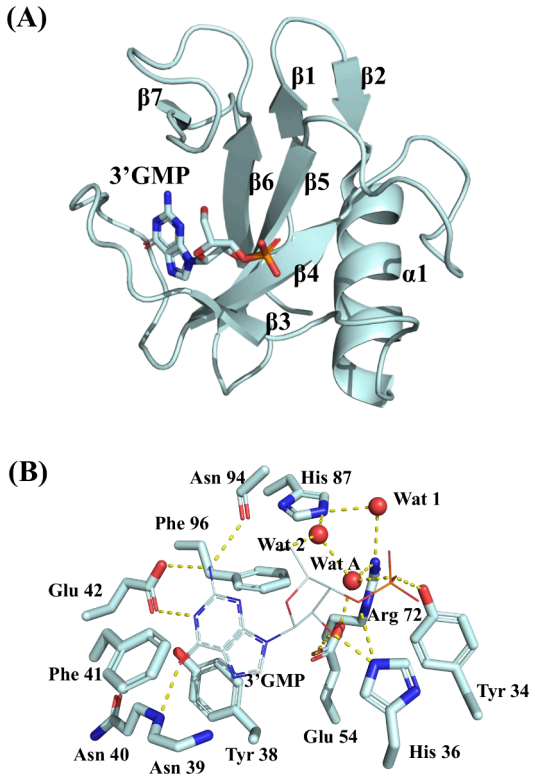

Figure 4. Overall structure of the Po1 and 3′GMP complex. (A) 3D view of the overall structure of RNase Po1/3′GMP complex (B) Active center view of RNase Po1. The yellow dotted line indicates the hydrogen bond.

Structural Comparison with the Apo Form

The structural comparison between the Po1 apo form and 3′GMP complex revealed a root-mean-square deviation (rmsd) value of 0.240 Å in the main chain. In the guanosine binding site of the 3′GMP complex, notable shifts were observed in the side chain of Tyr38 and Phe41, Glu42 flipping, and a shift in the carbonyl base of the main chain in Asn94. Additional structural variances were noted in the α1-β3 and β5-β6 loops. Notably, these loops are in the proximity of other Po1 molecules within the crystal lattice, hinting at potential influences from crystal packing effects. A water molecule (Wat A) forming hydrogen bonds with Tyr34, Glu54, and Arg72 in the active center was conserved in both complexes (Figure 5A).

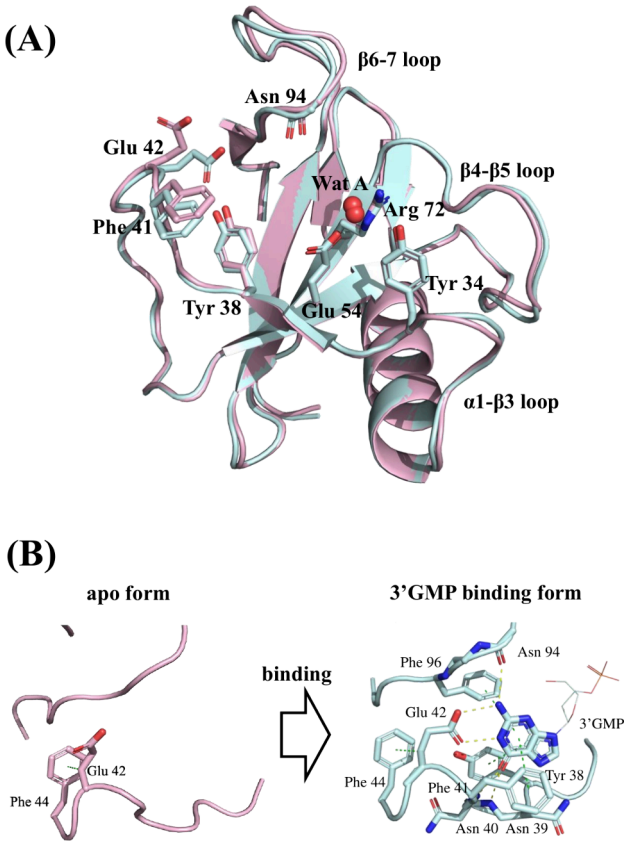

Figure 5. Structural comparison of the apo form and the Po1/3′GMP complex. (A) Po1 apo form: pink; Po1/3′GMP: cyan. Tyr38, Phe41, Glu42, and Asn94 changed the binding form of 3′GMP. Wat A was conserved in the apo form and the Po1/3′GMP complex. (B) 3D view of the base recognition residues being changed. The green dotted lines indicate hydrophobic interactions, and the yellow dotted lines indicate hydrogen bond interactions.

Recognition Mechanism of 3′GMP

We focused on Glu42, which exhibited a different conformation between the apo form and the 3′GMP complex. In the apo form, Glu42 exhibited only CH/π interaction using the alkyl chain moiety of the side chain to interact with the benzyl group in the side chain of Phe44 (Figure 5B). Contrastingly, in the 3′GMP binding form, Glu42 formed hydrogen bonds with the nitrogen atom at position 1 and the

https://doi.org/10.1021/acsbiomedchemau.4c00046
ACS Bio Med Chem Au 2024, 4, 257−267

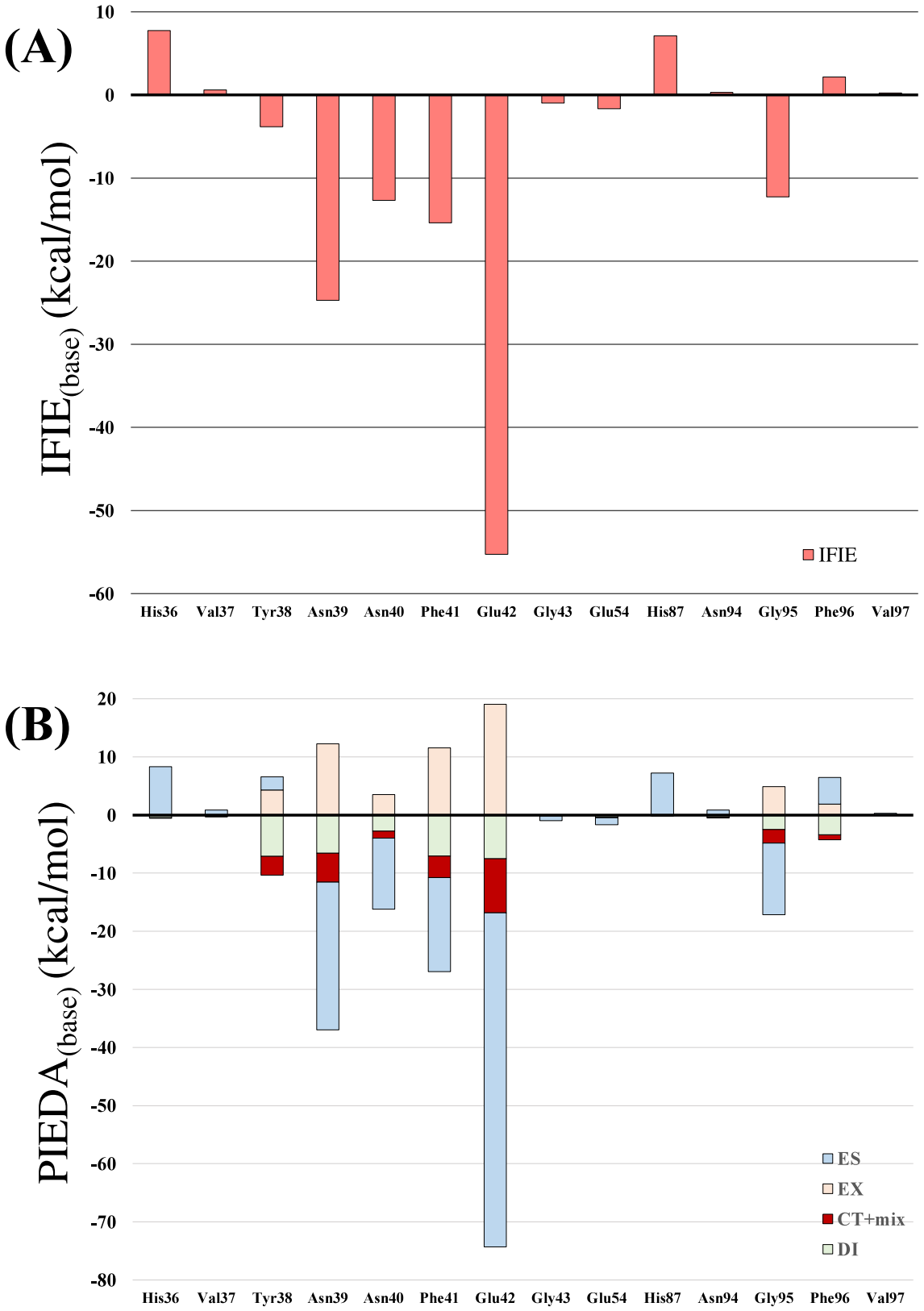

Figure 6. Conformational changes and the interaction energy to bind to the base of 3′GMP. (A) Bar graph represents the $IFIE_{(base)}$ results. (B) $PIEDA_{(base)}$ results are presented as a stacked bar chart. ES: electrostatic term, EX: exchange-repulsion term, CT+mix: charge transfer with higher-order mixed terms, DI: dispersion interaction term, IFIE: interfragment interaction energy.

amino group at position 2 of guanosine as well as hydrogen bonds with the nitrogen atom of the main chain of Phe96 (Figure 5B). The CH/π interaction between Glu42 and Phe44 was conserved. FMO calculations suggested that the $IFIE_{(base)}$ of Glu42 was −55.3 kcal/mol, with significant ES and CT+mix terms: − 57.5 and −9.3 kcal/mol, respectively. This indicates

https://doi.org/10.1021/acsbiomedchemau.4c00046
ACS Bio Med Chem Au 2024, 4, 257−267

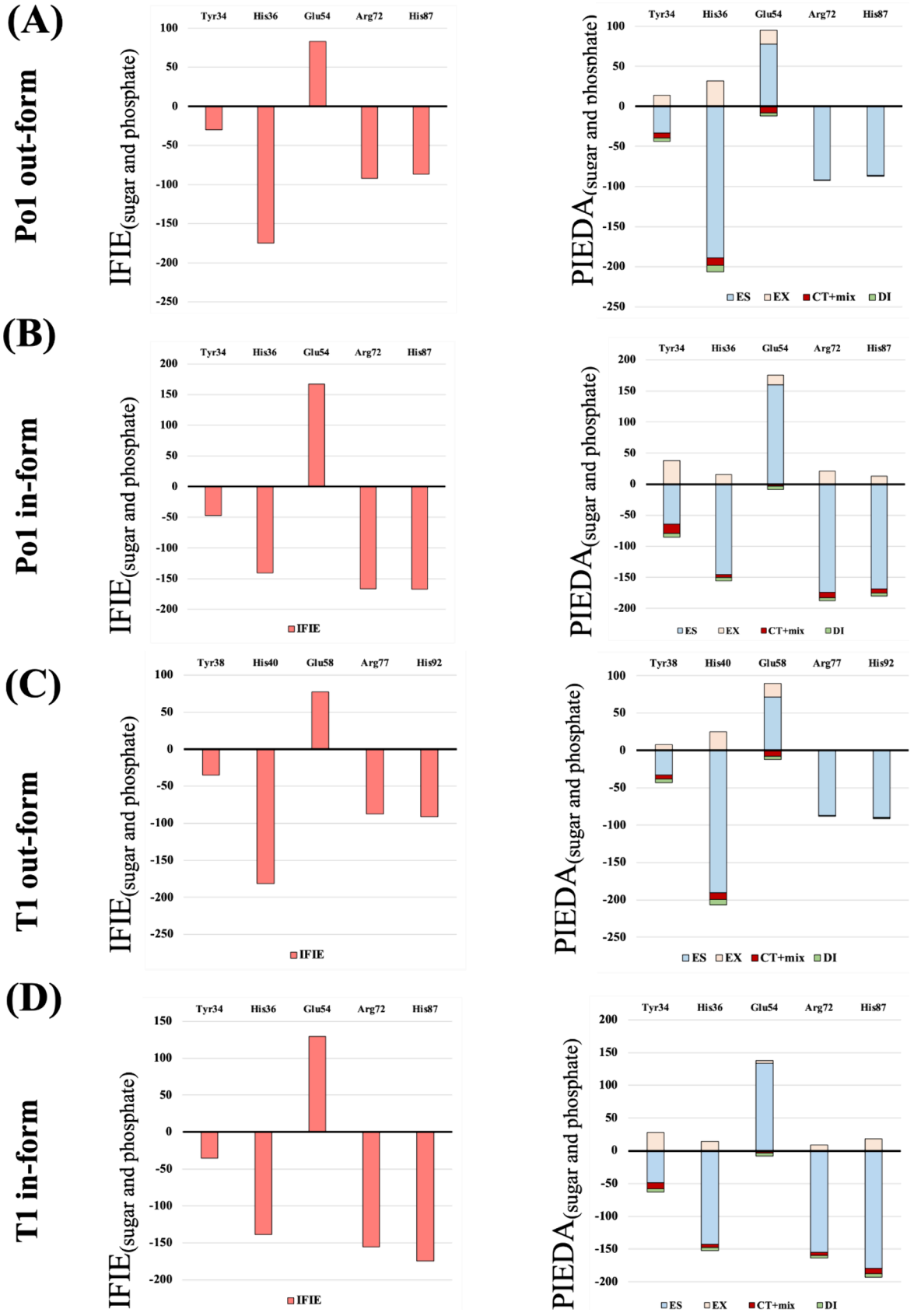

Figure 7. Interaction of the sugar and phosphate base in the out- and in-forms of Po1 and T1. The left panel shows the results of $IFIE_{(sugar\ and\ phosphate\ complex)}$. The right panel shows the results of $PIEDA_{(sugar\ and\ phosphate\ complex)}$. (A) Out-form of the Po1/3′GMP complex. (B) In-form of the Po1/3′GMP complex. (C) Out-form of the T1/3′GMP complex. (D) In-form of the T1/3′GMP complex.

https://doi.org/10.1021/acsbiomedchemau.4c00046
ACS Bio Med Chem Au 2024, 4, 257−267

that Glu42 was the most important residue contributing to the stability of 3′GMP binding through hydrogen bonding with guanosine bases (Figure 6A). Glu42 is important in forming the hydrogen bond network necessary for 3′-GMP base binding. In RNase T1, Glu46 (corresponding to Glu42 in Po1) was considered primarily responsible for guanine binding.[38] Our result presented here is consistent with the result of this previous study. We focused on other residues that exhibited different conformations between the apo form and 3′GMP. Tyr38 forms a $\pi-\pi$ stacking with the base moiety, Phe41 forms a CH/π stacking, and the results of DI term of $PIEDA_{(base)}$ suggested that Tyr38 (−7.1 kcal/mol) and Phe41 (−7.1 kcal/mol) were the most favorable residues among the base recognition sites. Thus, these residues were considered the most important in the dispersion interaction (Figure 6B). Additionally, the carbonyl group of the main chain of Asn94 (Gly95 fragment on the division of the FMO fragment) had the most favorable ES and CT+mix terms on the β6−7 loop (ES: − 12.3 kcal/mol and CT+mix: − 2.3 kcal/mol). FMO calculation highlighted the significance of residues that underwent conformational changes in their side chains to facilitate binding to 3′GMP, underscoring their importance in interaction dynamics.[39]

Type of the Binding Form of 3′GMP in the RNase T1 Family

In the structure of Po1/3′GMP, the phosphate base of 3′GMP was located away from His87. In the T1 family of the 3′GMP complexes, two types of 3′GMP binding modes existed. One was the phosphate base that formed a hydrogen bond with His87 and was located inside the active center (PDB ID: 6GSP), called the in-form (Figure 2B and D). The other is the phosphate moiety that did not form a hydrogen bond with His87 and was located away from the active center (PDB ID: 1GSP, 2GSP, 3GSP, 4GSP, 5GSP), called the out-form (Figure 2A and C).

Stability of 3′GMP

Within the RNase T1 family, the 3′GMP binding form exhibited division into two distinct forms. The interaction between the 3′GMP and side chain near the active center was evaluated by FMO calculation in in-form and out-of-form models of Po1/3′GMP and T1/3′GMP from the quantum chemical point of view. In Po1, the total $IFIE_{(3'GMP)}$ was −502.3 kcal/mol in the in-form and −657.3 kcal/mol in the out-form. Contrastingly, in T1, the total $IFIE_{(3'GMP)}$ of all fragments containing only protein was −323.7 kcal/mol in the in-form and −198.0 kcal/mol in the out-form. The $IFIE_{(3'GMP)}$ value indicated a favorable interaction between 3′GMP and both forms of T1 and Po1.

Active Center of RNase Po1 and T1

In a previous study, the catalytic residues of RNase T1 were glutamic acid on β4, arginine on β5, and histidine on β6-β7, and the role of histidine on the β3 sheet was explored as either a catalytic residue or one of the general bases. Therefore, we investigated the interaction of T1 and Po1 with sugar and phosphate fragments, which is the most relevant for RNase activity in 3′GMP.

RNase Po1. In the catalytic pocket, the $IFIE_{(sugar\ and\ phosphate)}$ value indicated that Tyr34, His36, Arg72, and His87 were favorable in both forms, and Glu54 was unfavorable in the out-form and favorable in the in-form (Figure 7A, B). In the out-of-form model, the favorable interaction with 3′GMP by Arg72 and His87 mostly consisted of the ES term, while in the in-form model, other terms contributed. The $IFIE_{(sugar\ and\ phosphate)}$ of Glu54 was 166.9 kcal/mol in the in-form model and 82.8 kcal/mol in the out-form. The side chain of Glu54 was the deprotonated state of the carboxylate group in the in- and out-of-form model (Figure 7A, B). His36 was more favorable in both forms (In-form: −140.4 kcal/mol, out-form: −174.5 kcal/mol) and in the ES, CT+mix, and DI terms. In the in-form model, $PIEDA_{(sugar\ and\ phosphate)}$ indicated that Tyr34 exhibited the largest CT+mix energy value in catalytic residues and Tyr34 was also favorable in the ES and DI terms in both forms.

RNase T1. In the catalytic pocket, $IFIE_{(sugar\ and\ phosphate)}$ indicated that Tyr38, His40, Arg77, and His92 were favorable, whereas Glu58 was unfavorable in the in- and out-form (Figure 7C and D). Both the in-form and out-form models exhibited the same tendencies as Po1. Arg77 and His92 were primarily composed of the ES term; however, in the in-form model, both residues were favorable in ES, CT+mix, and the DI term. The $IFIE_{(sugar\ and\ phosphate)}$ of Glu58 was 129.7 kcal/mol in the in-form model and 77.0 kcal/mol in the out-form model. The $IFIE_{(sugar\ and\ phosphate)}$ of His40 exhibited a favorable interaction with a value of −143.7 kcal/mol in the in-form model and −181.5 kcal/mol in the out-form model. The $PIEDA_{(sugar\ and\ phosphate)}$ of Tyr38 exhibited the most favorable interaction in the CT+mix term in all catalytic residues, and Tyr38 was also favorable in the ES and DI terms in both forms.

Role of Glutamic Acid on the β4 Sheet and Histidine on the α1-β3 Loop

To demonstrate RNase activity, the 2′-O atom of ribose must be deprotonated in the reaction mechanism. We considered two models. One model involved the deprotonation of glutamic acid (Po1:Glu54/T1:Glu58) and required the histidine (Po1:His36/T1:His40) to be in the biprotonated (HIP) conformation. The other model involved the protonation of glutamic acid (Po1:Glu54/T1:Glu58) and the neutralization of the histidine (His36/His40), with the δ-nitrogen being protonated (HID) in the conformation.

In Po1, comparing the total energy between the HIP (His36)/deprotonated glutamic acid (Glu54) model and the HID (His36)/protonated glutamic acid (Glu54) model indicated that the HIP (His36)/deprotonated glutamic acid (Glu54) model was 137.8 kcal/mol more stable than the HID (His36)/protonated glutamic acid (Glu54) model. Therefore, the Glu54 (deprotonated)/HIP (His36) model is considered to be more promising than the Glu54 (protonated)/HID model.

The His40Ala mutation was lost, and the His40Lys mutation partially conserved the RNase activity.[13,15] This histidine formed a favorable interaction of 3′GMP with ES, CT+mix, and the DI term. Lysine is a polar amino acid and might form favorable interactions with the ES and CT+mix term and 3′GMP as in histidine. Contrastingly, the lysine is inferior to histidine regarding side-chain stability (for example, CH/π interaction). Hence, His40Lys T1 would exhibit partially conserved RNase activity when compared to Native T1. However, histidine on the β3 sheet strongly interacted with 3′GMP in all residues; therefore, this histidine was an essential catalytic residue, as previously reported by Arni et al.[10] The deprotonated side chain of glutamic acid (Glu54) in the out-form appears to be highly unfavorable for phosphate bonding. However, a water molecule (WatA) can stabilize Glu54 in its

https://doi.org/10.1021/acsbiomedchemau.4c00046
ACS Bio Med Chem Au 2024, 4, 257−267

deprotonated state by forming a hydrogen bond with the active center of Glu54. Glu54, in its deprotonated state, is beneficial for withdrawing the hydrogen from the 2′-O atom of ribose, transitioning into the in-form, and exhibiting RNase activity.

Role of Tyrosine in the α1-β3 Loop

Tyrosine in the α1-β3 loop interacts with 3′GMP and histidine on the β3 sheet.

The well-conserved tyrosine in the α1-β3 loop (Po1:Tyr34, T1:Tyr38) in the RNase T1 family is situated in the active center but has not been considered to be a catalytic residue. The $IFIE_{(sugar\ and\ phosphate)}$ of Tyrosine (Po1:Tyr34, T1:Tyr38) in the in-form of Po1 is −47.5 kcal/mol (ES term: −64.1 kcal/mol, CT+mix term: −15.3 kcal/mol, DI term: −5.7 kcal/mol), and the in-form of T1 is −35.2 kcal/mol (ES term: −48.5 kcal/mol, CT+mix term: −9.8 kcal/mol, and DI term: −4.5 kcal/mol). The $IFIE_{(sugar\ and\ phosphate)}$ of Tyrosine (Po1:Tyr34, T1:Tyr38) in the out-form of Po1 is −30.0 kcal/mol (ES term: −33.2 kcal/mol, CT+mix term: −6.1 kcal/mol, DI term: −4.4 kcal/mol), and the out-form of T1 is −34.9 kcal/mol (ES term: −31.1 kcal/mol, CT+mix term: −5.5 kcal/mol, and DI term: −4.2 kcal/mol) (Figure 7A−D). These results indicate that the tyrosine (Po1:Tyr34/T1:Tyr38) on the α1-β3 loop forms favorable hydrogen interactions with $-0.06e \sim 0.11e$ charge transferred to 3′GMP in both forms. This is supported by FMO calculations, underscoring the crucial role of tyrosine on the α1-β3 loop in driving the RNase reaction. Additionally, this tyrosine engaged in $\pi-\pi$ stacking with the imidazole ring of histidine (Po1:His36/T1:His40) on the β3 sheet, displaying favorable interactions with the dispersion interaction terms. As previously mentioned, this histidine was deemed to be crucial to the RNase reaction. Moreover, the tyrosine on the α1-β3 loop fixes and determines the conformation of the histidine side chain on the β3 sheet, potentially stabilizing the RNase activity.

In addition to the active center, binding to the subsite where base binding occurs is also important when considering RNase activity. Currently, structures reported with binding to the subsite are RNase Ms of *Aspergillus phoenicis* (PDBID: 1RDS) and RNase T1 of *Aspergillus oryzae* (PDBID: 1B2M/2RNT/1RGA). RNase Ms and RNase T1 have been reported to have a structure where 3′GMP is bound to the active center, similar to Po1 in this study. Comparing the structure of RNase/RNA analog binding in the active center and subsite with RNase/3′GMP, it was indicated that all the catalytic residues were structurally conserved. Based on the above, we believe that the activity mechanism discussed in this study, along with the novel catalytic residue Tyr34, could be applied to the degradation mechanism of single-stranded RNA.

RNase Activity and Stability of the Single-Point Mutation Y34F Po1

Expression of a single-point mutated Y34F Po1 in *E. coli* provided approximately 3,600 units (~6.9 mg) in 1.9 L of culture supernatant. Y34F Po1 was homogeneous, as shown by SDS-PAGE (Figure 3(2)). The single-point mutated Po1 Y34F exhibited a minimal difference in the optimum enzyme temperature compared to the wild-type Po1 (Figure 8A). In RNase Po1, the side chain of Tyr34 engages in hydrophobic interactions with His36, Glu54, Pro56, Pro68, and Arg72, with no hydrogen bonds except for the one in the water molecule. These hydrophobic interactions are presumed to be conserved in Phe34, suggesting that this point mutation in Po1 contributes to little difference in structural stability. Nevertheless, the RNase activity of the single-point mutation Po1 decreased by 80% compared to that of wild-type Po1, indicating that tyrosine in the α1-β3 loop was the catalytic residue (Figure 8B).

(A)

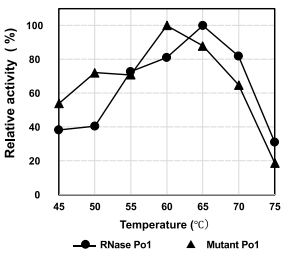

(B)

RNase	Optimum pH	Optimum temperature (°C)	Specific activity (units/mg)
RNase Po1	7.5	65	1957
Mutant Po1	7.5	60	474

Figure 8. Effects of temperature on the enzymatic activity of RNase Po1 and the mutant Po1. Upper graph: Enzymatic activity was determined as described in the text (0.01 M) using RNA as the substrate at pH 7.5 and incubation for 5 min at various temperatures. Symbols: ●, RNase Po1; ▲, Mutant Po1. Lower table: Enzymatic properties of RNase Po1 and the mutant Po1 Optimum pH: Enzymatic activity was determined as described in the text (0.01 M) using RNA as the substrate. The buffers (0.01 M) used were acetate-NaOH buffer at 5.5−6.5 pH and Tris-HCl buffer at 6.0−8.5 pH. Optimum temperature: Enzymatic activity was determined as described in the text (0.01 M) using RNA as the substrate at pH 7.5 and incubation for 5 min at various temperatures. Specific activity: Enzymatic activity was determined as described in the text (0.01 M) using RNA as substrate at pH 7.5. Protein concentration was determined as described in the text using a Pierce BCA Protein Assay Kit using bovine serum albumin as a standard.

Effect of Mutation (Y34F) on Antitumor Activity

We have revealed that RNase Po1 exhibits antitumor activity in blood cancer cell lines.[4] While RNase T1 has the same catalytic residues and protein size as RNase Po1, it lacks antitumor activity. The key distinction lies in the distribution of surface charges, with Po1 being positively charged[3] but T1 being negatively charged. In the present study, cell proliferation assays revealed that the mutated Po1 (Y34F) resulted in a 10−20% decrease in inhibition of HL-60 cell proliferation compared to the native Po1 (Figure 9). Despite no difference in surface charge, the mutated Po1 (Y34F) exhibited decreased antitumor efficacy, suggesting that RNase activity directly impacts its antitumor effects. In the RNase T1 family, α-sarsin shares antitumor activity with Po1. Structural superposition with Po1 revealed the conservation of catalytic residues, including histidine, glutamic acid, arginine, and tyrosine (a newly identified catalytic residue). Despite the difference in overall structure between α-sarsin and Po1, these common residues suggest that RNase activity could also be crucial for the antitumor activity of α-sarsin. However, RNase activity alone cannot account for all of the antitumor effects. The

https://doi.org/10.1021/acsbiomedchemau.4c00046
ACS Bio Med Chem Au 2024, 4, 257−267

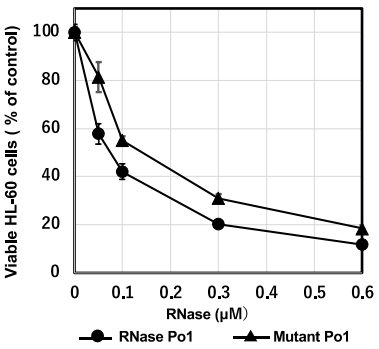

Figure 9. Effects of RNase Po1 and the mutant Po1 on the proliferation of HL-60 cells were determined using the 3-[4,5-dimethylthiazol-2-yl]-2,5 diphenyl tetrazolium bromide assay. Each point is the mean of three replicates and is reported as a percentage of the control that lacked RNase. Cells were treated with an indicated concentration of RNase Po1 or the mutant Po1 for 72 h. Cell proliferation without RNase was normalized to 100%. Symbols: ●, RNase Po1; ▲, Mutant Po1.

antitumor activity of RNase Po1 may also be influenced by the amount of cellular uptake. Furthermore, it is necessary to confirm the change in cellular uptake of RNase Po1 due to the mutation (Y34F).

CONCLUSION

The Po1/3′GMP complex structure was solved at a resolution of 1.75 Å. The studies involving crystal structure and FMO calculations elucidated that in recognizing the base of 3′GMP, Glu42 was the most important residue in terms of the hydrogen bond and Tyr38 and Phe41 were the most important residues in terms of dispersion interactions. Phe44 formed a CH/π interaction with Glu42 and was conserved between the apo and the 3′GMP binding forms. The 3′GMP forms two stable states that differ from the phosphate base when binding to the RNase T1 family. The in- and out-form combination of the Po1/3′GMP and T1/3′GMP indicated that the tyrosine (Po1: Tyr34/T1:Tyr38) located on the α1-β3 loop was a new candidate for the active residue. Additionally, in the active center, deprotonated glutamic acid (Po1: Glu54/T1: Glu58) and the biprotonated histidine (Po1: His36/T1: His40) were advantageous for RNase activity. The one-point mutation of Y34F Po1 decreased the RNase-specific activity by 75% and the antitumor activity by 10−30% in the leukemia cell line. This result confirms that the tyrosine on β3 serves as a catalytic residue and that RNase activity is linked to antitumor effects. Additionally, comparing the apo form of Po1 with that of the Po1/3′GMP complex indicated that the water molecules assisted in anchoring the catalytic residues to form the hydrogen bonds, potentially facilitating the reaction progression by successively replacing the water with a phosphate ion in the active center.

ASSOCIATED CONTENT

Data Availability Statement

The atomic coordinates and structure factors (PDB ID code 3WR2) were deposited in the Worldwide Protein Data Bank (http://www.wwpdb.org/). The accession number of the nucleotide sequence of cDNA for RNase Po1 is AB429298. The structure of the Po1/3′GMP complex was deposited in PDB (PDB ID:3WR2), and the FMO calculation was deposited in FMODB.[40] (FMODB ID: the Po1/3′GMP complex (out-form): 5NRRZ, Po1/3′GMP complex (in-form): YN9N2, the T1/3′GMP complex (out-form): K2KK3, and Po1/3′GMP complex (in-form): 4LQQN.)

Supporting Information

The Supporting Information is available free of charge at https://pubs.acs.org/doi/10.1021/acsbiomedchemau.4c00046.

Summary of data collection and refinement (PDF)

AUTHOR INFORMATION

Corresponding Author

Hiroko Kobayashi − *School of Pharmacy, Nihon University, Funabashi, Chiba 274-8555, Japan;* orcid.org/0000-0002-1660-0575; Phone: +81 047 465 4584; Email: kobayashi.hiroko@nihon-u.ac.jp

Authors

Katsuki Takebe − *Department of Dental Pharmacology, Faculty of Medicine, Dentistry and Pharmaceutical Sciences, Okayama University, Okayama 700-8525, Japan*

Mamoru Suzuki − *Institute for Protein Research, Osaka University, Suita, Osaka 565-0871, Japan*

Yumiko Hara − *Institute for Protein Research, Osaka University, Suita, Osaka 565-0871, Japan*

Takuya Katsutani − *Institute for Protein Research, Osaka University, Suita, Osaka 565-0871, Japan*

Naomi Motoyoshi − *School of Pharmacy, Nihon University, Funabashi, Chiba 274-8555, Japan*

Tadashi Itagaki − *School of Pharmacy, Nihon University, Funabashi, Chiba 274-8555, Japan*

Shuhei Miyakawa − *Graduate School of Pharmaceutical Sciences, Osaka University, Osaka 565-0871, Japan*

Kuniaki Okamoto − *Department of Dental Pharmacology, Faculty of Medicine, Dentistry and Pharmaceutical Sciences, Okayama University, Okayama 700-8525, Japan*

Kaori Fukuzawa − *Graduate School of Pharmaceutical Sciences, Osaka University, Osaka 565-0871, Japan;* orcid.org/0000-0001-5357-8250

Complete contact information is available at: https://pubs.acs.org/10.1021/acsbiomedchemau.4c00046

Author Contributions

All authors have given approval to the final version of the manuscript.

Funding

This research is (partially) supported by the Platform Project for Supporting in Drug Discovery and Life Science Research (Platform for Drug Discovery, Informatics, and Structural Life Science) from the Ministry of Education, Culture, Sports, Science, and Technology (MEXT) and the Japan Agency for Medical Research and Development (AMED) (Proposal No. 2012G001, 2013R-11). This work was performed with the approval of the Photon Factory Program Advisory Committee (Proposal No. 2017G148). This work was partly performed under the Collaborative Research Program of the Institute for Protein Research, Osaka University, CR-15−05, CR-16−05, CR-17−05, and CR-18−05. The FMO calculations were performed under the activities of the FMO drug design

consortium (FMODD) using the Fugaku supercomputer (project ID: hp230131).

Notes

The authors declare no competing financial interest.

■ ACKNOWLEDGMENTS

We thank Dr. Ryuichi Kato for helping with the experiments related to the crystallization of the 3′-GMP−RNase Po1 complex.

■ REFERENCES

(1) Yoshida, H. The Ribonuclease T1 Family. *Methods Enzymol.*; Nicolson, A. W., Ed.; Academic Press: New York. 2001, *341*, 28−41.
(2) Nomura, H.; Inokuchi, N.; Kobayashi, H.; Koyama, T.; Iwama, M.; Ohgi, K.; Irie, M. Purification and Primary Structure of a New Guanylic Acid Specific Ribonuclease From Pleurotus ostreatus. *J. Biochem.* **1994**, *116*, 26−33.
(3) Kobayashi, H.; Katsutani, T.; Hara, Y.; Motoyoshi, N.; Itagaki, T.; Akita, F.; et al. X-ray Crystallographic Structure of RNase Po1 That Exhibits Anti-tumor Activity. *Biol. Pharm. Bull.* **2014**, *37*, 968−978.
(4) Kobayashi, H.; Motoyoshi, N.; Itagaki, T.; Tabata, K.; Suzuki, T.; Inokuchi, N. The Inhibition of Human Tumor Cell Proliferation by RNase Po1, a Member of the RNase T1 Family, From *Pleurotus ostreatus*. *Biosci. Biotechnol. Biochem.* **2013**, *77*, 1486−1491.
(5) Olson, B. H.; Goerner, G. L. Alpha Sarcin, a New Antitumor Agent. I. Isolation, Purification, Chemical Composition, and the Identity of a New Amino Acid. *Appl. Microbiol.* **1965**, *13*, 314−321.
(6) Sacco, G.; Drickamer, K.; Wool, I. G. The Primary Structure of the Cytotoxin Alpha-Sarcin. *J. Biol. Chem.* **1983**, *258*, 5811−5818.
(7) Arni, R; Heinemann, U; Tokuoka, R; Saenger, W Three-Dimensional Structure of the Ribonuclease T1 2′-GMP Complex at 1.9-A Resolution. *J. Biol. Chem.* **1988**, *263*, 15358−15368.
(8) Nonaka, T.; Nakamura, K. T.; Uesugi, S.; Ikehara, M.; Irie, M.; Mitsui, Y. Crystal Structure of Ribonuclease Ms (as a Ribonuclease T1 Homologue) Complexed With a Guanylyl-3′,5′-Cytidine Analogue. *Biochemistry.* **1993**, *32*, 11825−11837.
(9) Noguchi, S.; Satow, Y.; Uchida, T.; Sasaki, C.; Matsuzaki, T. Crystal Structure of Ustilago Sphaerogena Ribonuclease U2 at 1.8 A Resolution. *Biochemistry.* **1995**, *34*, 15583−15591.
(10) Arni, R.; Heinemann, U.; Tokuoka, R.; Saenger, W. Three-Dimensional Structure of the Ribonuclease T1 2′-GMP Complex at 1.9-A Resolution. *J. Biol. Chem.* **1988**, *263*, 15358−15368.
(11) Takebe, K.; Suzuki, M.; Sangawa, T.; Motoyoshi, N.; Itagaki, T.; Kashima, K.; Uzawa, N.; Kobayashi, H. Identification of the Acidification Mechanism of the Optimal pH for RNase He1. *Biol. Pharm. Bull.* **2023**, *46*, 1778−1786.
(12) Ishikawa, K.; Suzuki, E.; Tanokura, M.; Takahashi, K. Crystal Structure of Ribonuclease T1 Carboxymethylated at Glu58 in Complex With 2′-GMP. *Biochemistry.* **1996**, *35*, 8329−8334.
(13) Koellner, G.; Choe, H. W.; Heinemann, U.; Grunert, H. P.; Zouni, A.; Hahn, U.; Saenger, W. His92Ala Mutation in Ribonuclease T1 Induces Segmental Flexibility. An X-ray Study. *J. Mol. Biol.* **1992**, *224*, 701−713.
(14) Steyaert, J.; Hallenga, K.; Wyns, L.; Stanssens, P. Histidine-40 of Ribonuclease T1 Acts as Base Catalyst When the True Catalytic Base, Glutamic acid-58, Is Replaced by Alanine. *Biochemistry.* **1990**, *29*, 9064−9072.
(15) Zegers, I.; Verhelst, P.; Choe, H. W.; Steyaert, J.; Heinemann, U.; Saenger, W.; Wyns, L. Role of histidine-40 in Ribonuclease T1 Catalysis: Three-Dimensional Structures of the Partially Active His40Lys Mutant. *Biochemistry.* **1992**, *31*, 11317−11325.
(16) Ardelt, W.; Mikulski, S. M.; Shogen, K. Amino Acid Sequence of an Anti-tumor Protein From Rana pipiens Oocytes and Early Embryos. Homology to Pancreatic Ribonucleases. *J. Biol. Chem.* **1991**, *266*, 245−251.
(17) Titani, K.; Takio, K.; Kuwada, M.; Nitta, K.; Sakakibara, F.; Kawauchi, H.; Takayanagi, G.; Hakomori, S. Amino Acid Sequence of Sialic Acid Binding Lectin From Frog (*Rana catesbeiana*) Eggs. *Biochemistry.* **1987**, *26*, 2189−2194.
(18) Kamiya, Y.; Oyama, F.; Oyama, R.; Sakakibara, F.; Nitta, K.; Kawauchi, H.; Takayanagi, Y.; Titani, K. Amino Acid Sequence of a Lectin From Japanese Frog (*Rana japonica*) Eggs. *J. Biochem.* **1990**, *108*, 139−143.
(19) Kitaura, K.; Ikeo, E.; Asada, T.; Nakano, T.; Uebayasi, M. Fragment Molecular Orbital Method: an Approximate Computational Method for Large Molecules. *Chem. Phys. Lett.* **1999**, *313*, 701−706.
(20) Huang, H. C.; Wang, S. C.; Leu, Y. J.; Lu, S. C.; Liao, Y. D. The Rana Catesbeiana Rcr Gene Encoding a Cytotoxic Ribonuclease. Tissue Distribution, Cloning, Purification, Cytotoxicity, and Active Residues for RNase Activity. *J. Biol. Chem.* **1998**, *273*, 6395−6401.
(21) Irie, M. Isolation and Properties of a Ribonuclease From Aspergillus saitoi. *J. Biochem.* **1967**, *62*, 509−518.
(22) Schägger, H.; von Jagow, G. Tricine-Sodium Dodecyl Sulfate-Polyacrylamide Gel Electrophoresis for the Separation of Proteins in the Range From 1 to 100 kDa. *Anal. Biochem.* **1987**, *166*, 368−379.
(23) Haider, S. R.; Reid, H. J.; Sharp, B. L. Tricine-SDS-PAGE. *Methods Mol. Biol.* **2012**, *869*, 81−91.
(24) Nitta, K.; Ozaki, K.; Ishikawa, M.; Furusawa, S.; Hosono, M.; Kawauchi, H.; Sasaki, K.; Takayanagi, Y.; Tsuiki, S.; Hakomori, S. Characterization of a Rana catesbeiana lectin-resistant mutant of leukemia P388 cells. *Cancer Res.* **1994**, *54* (4), 928−934.
(25) Otwinowski, Z.; Minor, W. Processing of X-ray Diffraction Data Collected in Oscillation Mode, Methods in Enzymology. *Macromol. Crystallogr. A*, Carter, C. W., Jr, Sweet, R. M., Eds., Academic Press: New York, 1997; Vol. *276*, pp 307−326.
(26) McCoy, A. J.; Grosse-Kunstleve, R. W.; Adams, P. D.; Winn, M. D.; Storoni, L. C.; Read, R. J. Phaser Crystallographic Software. *J. Appl. Crystallogr.* **2007**, *40*, 658−674.
(27) Murshudov, G. N.; Skubák, P.; Lebedev, A. A.; Pannu, N. S.; Steiner, R. A.; Nicholls, R. A.; et al. REFMAC5 for the Refinement of Macromolecular Crystal Structures. *Acta Crystallogr. D Biol. Crystallogr.* **2011**, *67*, 355−367.
(28) Adams, P. D.; Afonine, P. V.; Bunkóczi, G.; Chen, V. B.; Davis, I. W.; Echols, N.; et al.etal Phenix: a Comprehensive Python-Based System for Macromolecular Structure Solution. *Acta Crystallogr. D Biol. Crystallogr.* **2010**, *66*, 213−221.
(29) Emsley, P.; Cowtan, K. Coot: Model-Building Tools for Molecular Graphics. *Acta Crystallogr. D Biol. Crystallogr.* **2004**, *60*, 2126−2132.
(30) *Molecular Operating Environment (MOE)*; Chemical Publishing Computing Group ULC: Montreal, 2019.
(31) Frisch, M. J.; Trucks, G. W.; Schlegel, H. B.; Scuseria, G. E.; Robb, M. A.; Cheeseman, J. R. et al. *Gaussian16*, Revision A.03C.01; Gaussian, Inc.: Wallingford CT, 2016.
(32) Mochizuki, Y.; Tanaka, S.; Fukuzawa, K., Eds. *Recent Advances of the Fragment Molecular Orbital Method*; Springer: Singapore, 2021.
(33) Mochizuki, Y.; Nakano, T.; Koikegami, S.; Tanimori, S.; Abe, Y.; Nagashima, U.; Kitaura, K. A Parallelized Integral-Direct Second-Order Møller-Plesset Perturbation Theory Method With a Fragment Molecular Orbital Scheme. *Theor. Chem. Acc.* **2004**, *112*, 442−452.
(34) Mochizuki, Y.; Koikegami, S.; Nakano, T.; Amari, S.; Kitaura, K. Large Scale MP2 Calculations With Fragment Molecular Orbital Scheme. *Chem. Phys. Lett.* **2004**, *396*, 473−479.
(35) Fedorov, D. G.; Kitaura, K. Pair Interaction Energy Decomposition Analysis. *J. Comput. Chem.* **2007**, *28*, 222−237.
(36) Fukuzawa, K.; Tanaka, S. Fragment Molecular Orbital Calculations for Biomolecules. *Curr. Opin. Struct. Biol.* **2022**, *72*, 127−134.
(37) Zegers, I.; Loris, R.; Dehollander, G.; Fattah Haikal, A. F.; Poortmans, F.; Steyaert, J.; Wyns, L. Hydrolysis of a Slow Cyclic Thiophosphate Substrate of RNase T1 Analyzed by Time-Resolved Crystallography. *Nat. Struct. Biol.* **1998**, *5*, 280−283.
(38) Czaja, R.; Struhalla, M.; Höschler, K.; Saenger, W.; Sträter, N.; Hahn, U. RNase T1 Variant RV Cleaves Single-Stranded RNA After

https://doi.org/10.1021/acsbiomedchemau.4c00046
ACS Bio Med Chem Au 2024, 4, 257−267

Purines Due to Specific Recognition by the Asn46 Side Chain Amide. *Biochemistry*. **2004**, *43*, 2854−2862.
(39) Kobayashi, H.; Motoyoshi, N.; Itagaki, T.; Suzuki, M.; Inokuchi, N. Effect of the Replacement of Aspartic Acid/Glutamic Acid Residues With Asparagine/Glutamine Residues in RNase He1 From Hericium erinaceus on Inhibition of Human Leukemia Cell Line Proliferation. *Biosci. Biotechnol. Biochem.* **2015**, *79*, 211−217.
(40) Takaya, D.; Watanabe, C.; Nagase, S.; Kamisaka, K.; Okiyama, Y.; Moriwaki, H.; et al. FMODB: the World's First Database of Quantum Mechanical Calculations for Biomacromolecules Based on the Fragment Molecular Orbital Method. *J. Chem. Inf. Model.* **2021**, *61*, 777−794.

https://doi.org/10.1021/acsbiomedchemau.4c00046
ACS Bio Med Chem Au 2024, 4, 257−267